International Journal of Neural Systems, Vol. 30, No. 10 (2020) 2050057 (18 pages)

DOI: 10.1142/S0129065720500574

A Basal Ganglia Computational Model to Explain the Paradoxical Sensorial Improvement in the Presence of Huntington's Disease

Álvaro González-Redondo, Francisco Naveros, Eduardo Ros
and Jesús A. Garrido*,†
Department of Computer Architecture and Technology
University of Granada, Granada, Spain
†*jesusgarrido@ugr.es*

Accepted 30 June 2020
Published Online 24 August 2020

The basal ganglia (BG) represent a critical center of the nervous system for sensorial discrimination. Although it is known that Huntington's disease (HD) affects this brain area, it still remains unclear how HD patients achieve paradoxical improvement in sensorial discrimination tasks. This paper presents a computational model of the BG including the main nuclei and the typical firing properties of their neurons. The BG model has been embedded within an auditory signal detection task. We have emulated the effect that the altered levels of dopamine and the degree of HD affectation have in information processing at different layers of the BG, and how these aspects shape transient and steady states differently throughout the selection task. By extracting the independent components of the BG activity at different populations, it is evidenced that early and medium stages of HD affectation may enhance transient activity in the striatum and the substantia nigra pars reticulata. These results represent a possible explanation for the paradoxical improvement that HD patients present in discrimination task performance. Thus, this paper provides a novel understanding on how the fast dynamics of the BG network at different layers interact and enable transient states to emerge throughout the successive neuron populations.

Keywords: Basal ganglia; spiking neural networks; computational model; Huntington's disease; dopamine.

1. Introduction

Choosing the right action among many available options represents a primary but also challenging behavior for animal species. The basal ganglia (BG) have long been thought to play a pivotal role in the action selection process in the mammal brain.[1] A well-accepted hypothesis is that these nuclei choose between multiple motor commands coming from cortical areas.[2,3] However, it is still unclear how the BG filter incoming cortical commands in order to produce an accurate and fast output. This paper aims to explore the signal processing in the BG by embedding a computational model of this brain area in a behaviorally relevant experimental setting involving action selection.

The BG network presents complex anatomical and functional sub-divisions, but it is usually structured in five main neuron populations[4] which can be organized into following three sections (Fig. 1):

*Current address: Research Centre for Information and Communications Technologies (CITIC-UGR), Calle Periodista Rafael Gómez Montero 2, E18071 Granada, Spain.
†Corresponding author.

- The inputs of the BG are mainly received through the corpus striatum, with its main cell type being the medium spiny neurons (MSN), and the subthalamic nucleus (STN) neurons.
- The intermediate layers are composed by the external segment of the globus pallidus (GPe) and the substantia nigra pars compacta (SNc).
- The output projection to the thalamus is finally carried by the substantia nigra pars reticulate (SNr).

The connectivity of these populations is mainly drawn according to three main routes from the cortex to the thalamus as follows (Fig. 1):

- The direct pathway, where the cerebral cortex makes excitatory glutamatergic synapses into the MSN_{D1}, which inhibits the SNr.
- The indirect pathway, where the cerebral cortex excites the MSN_{D2}, which inhibits the GPe, and finally, the GPe which also inhibits the SNr.
- The hyper direct pathway, where the cortex makes glutamatergic connections into the STN, which diffusely excites the SNr.

In addition to these broad pathways, there are dopaminergic projections from the SNc to the MSN,

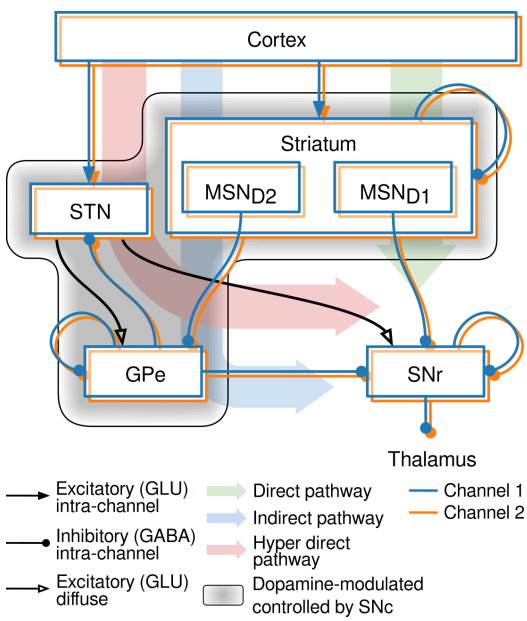

Fig. 1. (Color online) Computational model of the BG. BG representation structured in channels (blue and orange) showing the direct, indirect and hyper direct pathways.

the STN and the GPe with modulatory effects (shaded box in Fig. 1).[1,5] Finally, the GPe forms recurrent loops with the STN.

It has been hypothesized that the BG process a large number of cognitive streams or channels in parallel,[6,7] each of them representing a feasible action to be performed.[8] The BG are thought to act as an action selection machinery by inhibiting every nonselected action in the thalamus with the SNr, based on their corresponding activity level or salience.[3] A possible explanation for this mechanism was suggested by Ref. 1. They identified two steady-state and transient selection components, generated both in the striatum due to the cortex activity. According to this theory, the transient component in the striatum temporarily enhances the difference between several competing cortical inputs.

In order to shed some light on this action selection process, previous research in the literature has addressed both the natural and artificial alterations of the BG circuitry. For instance, the use of levodopa, a dopamine (DA) neurotransmitter precursor, modifies the levels of DA in the BG and systematically produces reduced reaction times and increased accuracy in simple auditory discrimination tasks in healthy subjects.[9] Additionally, several diseases can naturally affect the normal operation of the BG. This is the case of Huntington's disease (HD), which produces an enhanced activation of the N-methyl-D-aspartate (NMDA) glutamatergic receptors of the MSN in the striatum,[10] culminating in excitotoxicity (i.e. cell death).[11] Moreover, it is known that MSN expressing D2 dopaminergic receptors are more affected than those expressing D1 dopaminergic receptors in the early stages of HD,[12] disrupting the indirect pathway (MSN_{D2}-GPe-SNr). Finally, levodopa can potentiate the HD symptoms by exacerbating choreiform movements.[13] Despite these mainly negative effects of HD, some researchers have found a paradoxical improvement in auditory decision tasks (in both reaction time and accuracy) during early stages of the disease, presumably caused by the enhanced efficacy of NMDA receptors.[14] This improvement can help us to better understand both HD and the action selection process in the BG.[1]

Although different noninvasive experimental techniques and statistical analyses, such as electroencephalogram (EEG) and information metrics, allow

the identification of important brain areas related to specific tasks,[15,16] the way in which they contribute to complex behaviors remains highly elusive. In recent decades, the use of biologically inspired computational models emulating spiking neural networks[17] has been demonstrated as being useful for understanding experimental recordings from multiple brain areas[18,19] and for studying different neurological alterations.[20–22] Thus, computational models represent a promising approach to explore not only the normal operation of the BG, but also how different artificial alterations (e.g. levodopa) or diseases (e.g. HD[1] or Parkinson's disease (PD)[23,24]) can affect this nucleus. Although many computational models of the BG have been proposed to explain the overall operation of this brain area,[6,25–29] it remains unclear how the transient phenomena generated by the MSN[1] in the striatum on HD patients propagates to the SNr (BG output nucleus), how this transient phenomena facilitates action selection, and how DA affects this process.

In this paper, we present a computational model of the BG integrating all its main neuron types. This model facilitates the exploration of the emergence of both steady and transient phenomena in the MSN and the interplay between the three BG pathways in the propagation of these phenomena. In this framework, we have been able to quantify the selectivity between competing actions transmitted to the thalamus from the SNr output. In addition to this, we have explored how altered conditions, such as increased DA levels or the alterations produced by HD, affect the performance of the BG as selection machinery using a stimulus discrimination task as a test-bench.

Section 2 provides details on the implementation of the computational model. Section 3 describes the results emerging from the simulation of the computational model in the framework of the stimulus discrimination task. In Sec. 4, we discuss these results regarding previous computational models and experimental evidence in the literature. Finally, Sec. 5 summarizes the main contributions of this paper.

2. Computational Modeling of BG and HD

A computational model of the BG, including all its main nuclei and connections, has been implemented (Fig. 1). The network structure and the neuron models used in this paper are based on recent work by Fountas and Shanahan.[30] The model includes five neuronal populations and nine neuronal types (all of them implemented as Izhikevich neuron models, but with different parameters in order to capture their particular cell dynamics). The total number of simulated neurons is 5494 divided as follows: the MSN layer contains 2292 neurons, with half of them (1146) expressing D1 receptor and the other half D2 receptor. The STN layer contains 47 neurons, the GPe 155 neurons and the SNr 3000 neurons.

The neuron populations in our BG model have been connected following a channel structure. As a general norm, the neurons in every channel are only allowed to synapse neurons in the same channel. The exceptions are the STN efferents, which are diffuse and connect to all the channels (Fig. 1), and the lateral inhibition within and between the MSN channels and SNr channels. The modulatory connections from the SNc are considered implicitly as the global level of tonic DA in the model. The average level of activation (i.e. the firing rate) in each channel at the MSN represents the salience or urgency of the action represented at that particular channel.[31]

For the proposed selection task, we have implemented three different channels in our BG model following Ref. 1: one for the selected option (with 40% of the neurons), one for the nonselected option (with 40% of the neurons) and the third not competing in the selection task (with 20% of the neurons). The third channel represents background neuronal activity able to influence the other channels through the diffuse connectivity from STN and the lateral competition in MSN and SNr. For the sake of simplicity, only the selected (blue) and nonselected (orange) channels have been represented in the figures.

The following sections describe the behavior of the neuron models used, and the appendices go deeper into the modeling details. The source code of the model implementation for NEST 2.12,[32] as well as the scripts allowing the reproduction of the results shown in this paper, have been made available at the following address: https://github.com/EduardoRosLab/BG_selectivity.

2.1. *Neuron and synapse models*

The Izhikevich neuron model[33] has been chosen to reproduce the experimental firing modes recorded in the different neuron types of the BG. The parameters

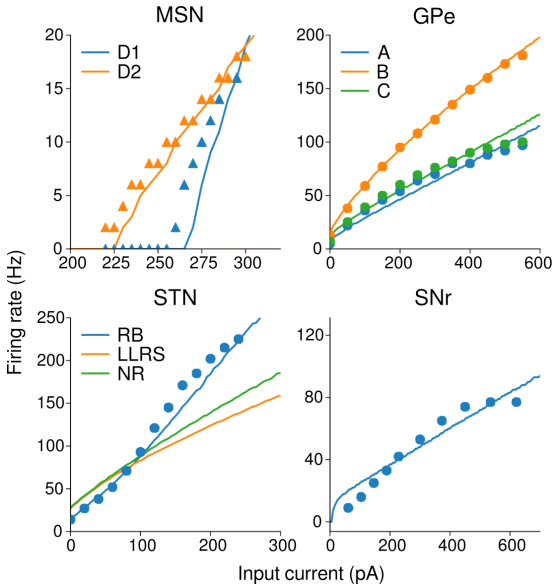

Fig. 2. Frequency–current (F–I) curves. Solid lines represent our computational results, while triangles and dots, respectively, represent the simulated and experimental data used to tune our models.

for each neuron type have been optimized following the adjustment procedure described in Ref. 34. This method aims to approximate electrophysiological properties (e.g. the action potential amplitude and width, the resting and threshold potentials and the rheobase current) and their steady-state frequency–current (F–I) relations. Figure 2 shows the reference and resulting F–I curves for each neuron type. We selected the parameters of our MSN (see https://github.com/EduardoRosLab/BG_selectivity/raw/master/parameters_tables.pdf in the repository) from different sources in order to obtain a good match between experimental data and simulated behavior, namely transient selectivity (see below). When the rest of the BG nuclei were added, their neuron model parameters were calculated following the previously described parameter estimation procedures[34] or by local search/manual tuning.

More than 90% of the striatal neurons are MSN, showing competitive behaviors between channels through lateral inhibition, both directly and through interneurons.[35] We modeled the striatum as a population of MSN with lateral inhibition. These neurons show characteristic firing patterns such as long-latency first spike following current injection or membrane potential bi-stability in response to random input activity, with a hyperpolarized down-state and depolarized up-state plateau.[28] Although other neuron types have been reported (e.g. diverse GABAergic populations[36] and cholinergic interneurons with a role in reinforcement-related signals[37]), we have intentionally ruled them out since our preliminary simulations showed that they did not impact the transitory effect under study in the proposed experimental setup. The MSN are divided into two subpopulations of 1146 neurons expressing different types of DA receptors (D1 and D2). Thus, two neuron types have been adjusted for the MSN subpopulation (see Appendix A for further details). Figure 2 shows the comparison of the F–I curves from our Izhikevich neuron models and the highly-detailed multi-compartment models of the MSN.[27]

Neurons in the GPe have shown at least two different firing patterns in primates: high-frequency discharge (HFD) separated by intervals of total silence and low-frequency discharge (LFD) and bursts.[38] Interestingly, similar intracellular recording in rats[39] has been reported to show three different identifiable firing patterns. In our model, we have followed this latter approach by including three neuron types named A, B and C.[34] Our model includes 131 neurons of type B, which behave similarly to HFD neurons (the only neuron type able to evoke rebound firing), and 7 and 17 neurons of types A and C, respectively, which behave similarly to LFD. Figure 2 shows the matching of the simulated neurons and the experimental data (dotted) from Ref. 39.

The STN is composed of three different neuron sub-types. All of them behave similarly when depolarized, with sigmoid F–I relation.[40] However, they have shown different responses after long depolarization, including rebound bursts (RB), long-lasting rebound spikes (LLRS) and no rebound (NR) effect. Our model, respectively, includes 28, 12 and 7 neurons of each cell type distributed between the three channels. Figure 2 includes experimental data (dots) for STN RB cell type from Ref. 40.

Finally, the GABAergic SNr neurons show spontaneous high-frequency firing that may turn abruptly into bursting or silence depending on external input. In addition to this, this type of neuron emits rebound spikes.[41,42] Our model includes 3000 SNr neurons, whose parameters have been adjusted to obtain firing rates around 20 Hz in absence of external current stimulation, and silent when the channel is selected. These firing rates fall within the range

obtained in cell recordings considered in other computational models.[37,43,44] Figure 2 shows a comparison of the firing rate of the simulated neuron and the experimental data for the SNr neuron type from Ref. 45.

All the neurons included in our BG model implemented chemical synapses. These were modeled using synaptic conductances governed by exponentially-decaying functions and constant synaptic weights (without plasticity mechanisms). Three types of chemical receptors with different temporal dynamics were implemented: AMPA, NMDA and $GABA_A$. The NMDA receptor also models the voltage-dependent magnesium plug.[46] In Table 1, we show the interconnectivity topology of our BG models. All the neurons implemented a probabilistic all-to-all connectivity distribution with connectivity ratios between neuron types extracted from literature.[1,34] These connections could be intra-channel (neurons just connected with neurons in the same channel) or inter-channels (neurons connected with neurons in the same or different channels). The rest of synaptic parameters were selected from the literature or obtained from local search/manual tuning. Details on the implementation can be found in Appendix B.

2.2. *Huntington's disease modeling*

HD has been demonstrated to disrupt the indirect pathway of the BG by reducing the number of MSN D2 neurons[12] during the early stages of the evolution of the disease. In our study we have modeled this effect by randomly removing a fraction of the MSN D2 neurons (Eq. (1)). Additionally, MSN D2 neurons also over-express NMDA receptors in early symptomatic and pre-symptomatic HD patients, leading to excessive action potential emission and eventually neuronal apoptosis.[47] This effect has been modeled by increasing the synaptic weight of NMDA receptors onto the MSN neurons (Eq. (2)).

$$n_{\mathrm{MSN}-D2} \leftarrow n_{\mathrm{MSN}-D2}(1 - \mathrm{hd} \cdot a_r), \tag{1}$$

$$w_{\mathrm{NMDA}} \leftarrow w_{\mathrm{NMDA}}(1 + \mathrm{hd} \cdot s_r), \tag{2}$$

where hd represents the level of HD ranging from zero (no HD effect) to one (maximum considered HD affectation), $n_{\mathrm{MSN}-D2}$ is the number of MSN neurons with DA receptor D2, a_r is the cell apoptosis ratio ranging from zero (no apoptosis) to one (maximum apoptosis), w_{NMDA} is the synaptic weight from cortex to MSN and s_r is the NMDA increase factor. The a_r and s_r parameters have been set to 0.8 and 1.0 since these values maximize the network effect during selection tasks according to previous research.[1] The combination of both effects simulates the early and middle stages of HD (grades one and two in the neuropathological scale proposed by Ref. 12). Finally, since advanced stages of HD are incompatible with behavioral experimentation (HD patients lose their motor control capabilities), modeling further damages in our BG model due to advanced stages of HD[48] remains beyond the scope of this work.

Table 1. Synaptic and connectivity parameters.

Connection	Receptor	Connectivity	Probability
Cortex → MSN	AMPA	Intra-channel	1.0
	NMDA	Intra-channel	1.0
MSN → MSN	$GABA_A$	Inter-channels	0.32
MSN → SNr	$GABA_A$	Intra-channel	0.033
SNr → SNr	$GABA_A$	Inter-channels	0.1
Cortex → STN	AMPA	Intra-channel	1.0
	NMDA	Intra-channel	1.0
STN → GPe	AMPA	Inter-channels	0.3
	NMDA	Inter-channels	0.3
GPe → STN	$GABA_A$	Intra-channel	0.1
GPe → GPe	$GABA_A$	Intra-channel	0.1
MSN → GPe	$GABA_A$	Intra-channel	0.033
STN → SNr	AMPA	Inter-channels	0.3
	NMDA	Inter-channels	0.3
GPe → SNr	$GABA_A$	Intra-channel	0.1066

3. Results

3.1. *Experimental framework*

HD patients show a paradoxical improvement (both in speed and precision) in the auditory decision task proposed by Beste.[14] In this experiment, the subject is told to distinguish between short (200 ms) and long (400 ms) auditory tones in a series by pressing a left or right button for each option (Fig. 3(a)).

The main inputs to the MSN and STN come from afferent axons of the pyramidal neurons in layer V from different cortex areas[49] (e.g. the auditory cortex[50]). This model assumes that the decision on the presented tone length, and its consequent motor action, has previously been performed in the cerebral cortex and propagated to the BG by modifying the firing rate of the input fibers that arrive to each BG channel. This cortical input activity has been

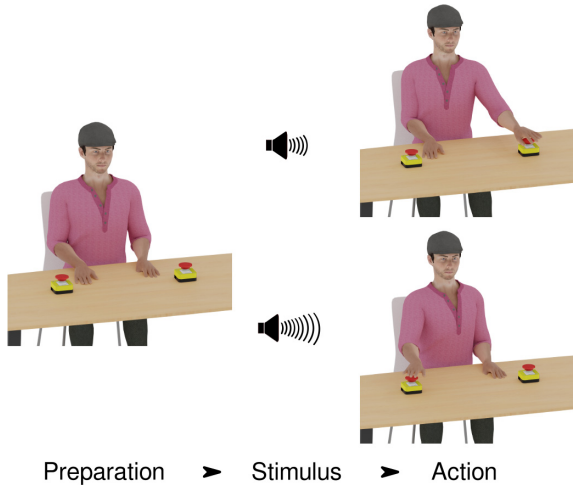

(a)

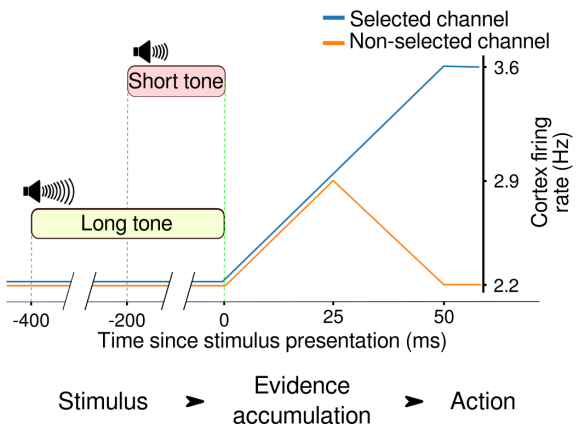

(b)

Fig. 3. Experimental framework. (a) Stimulus discrimination experimental procedure: The subject must press the left (right) button straight after a short (long) tone onset. (b) Firing rate evolution in the selected and nonselected channels in the cortex.

emulated by means of three populations of Poisson spike train generators emulating the cortical activity. These three populations project over the three channels in the MSN and STN (two channels for the left and right motor response, and a third channel processing cortical activity not related with the task). Thus, each neuron in MSN and STN receives the equivalent of 250 randomly-chosen input spike trains.[29]

The simulated protocol was taken from Ref. 1. It started with a stabilization period of 1500 ms in which the mean firing rate of the three Poisson populations was fixed to a baseline activity of 2.2 Hz. The end of this stabilization period corresponded with the end of the auditory stimulus. During the following 25 ms, the two Poisson populations corresponding with the short and long tones (press left and right button) gradually increased their mean firing rate to a medium excitation level of 2.9 Hz (Fig. 3(b)). After this 25 ms period, the subject was able to discriminate the tone length and select the corresponding motor action. During the next 25 ms, the Poisson population corresponding with the selected action kept increasing its firing rate until it reached an average firing rate of 3.6 Hz. On the contrary, the nonselected population returned to the baseline level of activity. These activation levels were maintained during an additional period of 1000 ms. Finally, the third Poisson population remained in the baseline state during the whole experiment (2550 ms). All these firing rates range within reported biological constraints for the auditory cortical layer.[51] Note that with this experimental protocol, we were not modeling the detection of longer tones (which were already encoded in the incoming cortex activity), but rather the selection of the action to be performed in response to the detection of short or long tones.

3.2. *Data analysis: Selectivity metrics*

The resulting action potentials obtained during the simulation of the model (each experiment lasting 2550 ms) were used to generate the activity histogram (1-ms bin) for each channel in every neuron population. The population spikes were filtered by convolving with a 7.5-ms Gaussian kernel to mimic the resulting excitation/inhibition received in the successive layer. Aiming to rule out the high variability of the resulting activity histograms, the instantaneous firing rate in each time bin has been averaged over 40 simulations with different random seeds for each experimental condition (Fig. 4(c)).

In order to provide a quantitative evaluation of the performance of the computational model in the proposed behavioral task, the following assumption has been made, which has been widely hypothesized before[2,6,7,52–54]: the BG chooses the action with the highest reward expectance between multiple possible actions by increasing (decreasing) the activity in the corresponding MSN (SNr) channel and reducing (maintaining) the firing rate in the remaining MSN (SNr) channels. Thus, the following estimators aim

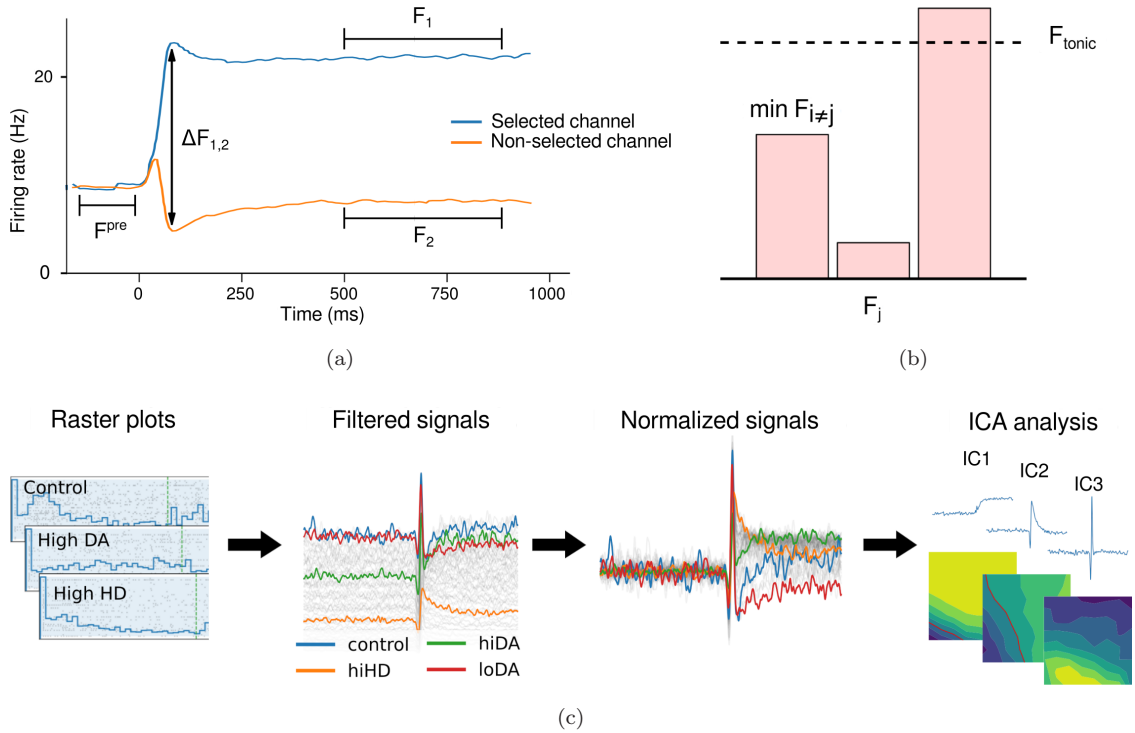

Fig. 4. (Color online) Analysis performed on the simulations results. (a) Selected (blue) and nonselected (orange) channel activities after the application of Gaussian kernels to the raster plot histograms (MSN or SNr). (b) Mean activity levels of the SNr channels before the tone onset (F_{tonic}) and after the tone onset (F_i, F_j), where F_j is the selected channel and F_i the nonselected one. (c) For the ICA analysis, the raster plot histograms are filtered, normalized and decomposed in their ICA components with their corresponding weights.

to quantify how distinguishable the activity profiles of the MSN and the SNr are in the considered channels.

Activity evaluation in the striatum: Selectivity

Following the approach in Ref. 1, the selectivity in the MSN can be defined as the ability to robustly distinguish competing signals. Two complementary modes of selectivity have been proposed, measured with different metrics applied to the mean activation of each MSN channel population. Given a competition between different cortical inputs, a transient selectivity is the temporary promotion of the most salient signal simultaneously to suppression of the least-salient signal. This effect results in the transient boost of the difference in salience between the competing signals. The transient selectivity in the MSN (TS_{MSN}) is defined according to

$$\text{TS}_{\text{MSN}} = 1 - \frac{\overline{F_1} - \overline{F_2}}{\Delta F_{1,2}}, \tag{3}$$

where F_1 and F_2 are two signals (firing rates of the two competing channels), $\Delta F_{1,2}$ is the maximum difference between F_1 and F_2 occurred during a transition window between 0 ms and 200 ms after the stimulation, and $\overline{F_1}, \overline{F_2}$ are the mean stable activity of signals F_1 and F_2 after the transition period (Fig. 4(a)).

Moreover, given a competition between different input signals, the least-salient signal (in our experiments, F_2) tends to be inhibited on a sustained basis by the most salient signal (Fig. 4(a)); this is called the stationary selectivity (SS_{MSN}) and is defined as follows:

$$\text{SS}_{\text{MSN}} = 100 \times \left(1 - \frac{\overline{F_2}}{\overline{F^{\text{Pre}}}}\right), \tag{4}$$

where $\overline{F^{\text{Pre}}}$ is the mean stable activity of the signal F_1 or F_2 before the tone onset (both activity level are similar before the stimulus onset). Thus, the TS_{MSN} provides an estimation of how distinguishable the competing signals are during the transitory state while the SS_{MSN} quantifies how distinguishable the

competing signals are once they have reached their steady state.

Activity evaluation in the SNr: Distinctiveness

A more general metric, which can be applied to the SNr, is the distinctiveness of a single selected channel, defined as the ability of a channel to generate distinctively less activity than any other channel in the layer.[34] Since the SNr inhibits the thalamus, the distinctive channel (the selected one with the lower activity) inhibits the corresponding channel in the thalamus in a lesser degree, propagating the BG selection to the thalamus. The distinctiveness in the SNr represents the degree to which the following two conditions are fulfilled: (a) the firing rate of the selected channel in the SNr is close to zero, and (b) no other channel is far below tonic levels. These two conditions can be quantitatively evaluated over the time t according to $a_j(t)$ and $b_j(t)$, respectively:

$$a_j(t) = 1 - \frac{F_j(t)}{\max\{F_{\text{tonic}}, F_j(t)\}}, \tag{5}$$

$$b_j(t) = \frac{\min F_{i\neq j}(t)}{\max\{F_{\text{tonic}}, \min F_{i\neq j}(t)\}}, \tag{6}$$

where j is the examined channel, $F_j(t)$ is the firing rate of channel j at time t, $\min F_{i\neq j}(t)$ is the minimum SNr firing rate of any channel different to j at time t and F_{tonic} is the tonic firing rate of the SNr, assumed here to be 20 spikes/sec (Fig. 4(b)). Then the distinctiveness $D_j(t)$ is defined as

$$D_j(t) = a_j(t) \cdot b_j(t), \tag{7}$$

where $D_j(t)$ values range in $[0, 1]$, with 1 indicating that the channel j at time t propagates distinctively less inhibition than any other channel to the thalamus, and 0 the opposite condition (or channel activity j is far from zero i.e. it is not chosen, or some other channel is closer to zero i.e. the other channel is chosen instead). The steady-state distinctiveness and transient distinctiveness[55] are both calculated from $D_j(t)$. The former is calculated as the average of the stable post-transient activity (the signal is assumed to reach steady state after 500 ms from the stimulus onset) while the latter is defined as the maximum distance between the distinctiveness of the channels during a fixed short interval (200 ms in our experiments) after the generation of the salient signal.

Independent component analysis

In order to evaluate the different temporal components emerging from the population activity, we have applied the independent component analysis (ICA) algorithm[56] to the filtered signal in the selected channel of the MSN (Fig. 4(c)). ICA is a widely used computational method for separating a multivariate signal into its additive nonorthogonal components. This is done by assuming that the subcomponents are non-Gaussian and statistically independent signals. Although this algorithm is similar to other classic methods, such as principal component analysis (PCA), ICA imposes to the resulting signals the harder constraint of being statistically independent (and not just linearly uncorrelated as in PCA). Based on preliminary simulations within the experimental setup under evaluation in this paper, ICA demonstrated to be more successful than the PCA on finding significant components.

Prior to the application of the ICA algorithm, each signal was normalized by subtracting the mean activation level before stimulus onset and the resulting signal was divided by its standard deviation, so that it becomes insensitive to any possible firing rate additive or multiplicative variation. After that, we used the fastICA decomposition function from the scikit-learn python library[57] to obtain the independent components from the signals. We chose the number of independent components to be at least two (as we make the assumption of the existence of the transient and the steady-state components) and as high as needed to be able to explain at least 90% of the variability of the signal. The same analysis was applied to both the selected and the nonselected channel populations of the SNr. Finally, the ICA algorithm provided the relative weights of each component in each experimental condition. The resulting weights allowed us to evaluate the presence and the relative importance of each temporal component for different combinations of factors.

3.3. *General network behavior*

Our network model was first simulated in control conditions (no HD hd = 0 and default level of DA $d_1 = d_2 = 0.3$) during Beste's task.[14] The resulting activity of each population and their respective channels are shown in Fig. 5. This activity falls within *in vivo* values in all nuclei: the MSN firing rates are

below 2 Hz when low activity and above 17 Hz in high activity.[34,44] The STN normally fires at around 10 Hz, but can get as high as 30–50 Hz.[58] The GPe firing rate is around 30 Hz without activation but raise to 40 Hz when its channel is not selected and decrease to almost zero when its channel is selected.[34] The SNr activity has been reported to be close to zero when receiving inhibition from MSN D1 and around 20–30 Hz when it is being activated.[34,44] Not surprisingly, the variability (standard deviation) of the population firing rate depends on the number of neurons included in each nucleus (ranging from 46 neurons in the GPe to 3000 neurons in the SNr). The initial 1500 ms are devoted to stabilizing the network activity in response to the basal activation in the cortex (Figs. 3(b) and 5). Some nuclei, such as the GPe and the SNr, show intrinsic activation, resulting in high firing rates at the beginning of the simulation that slowly decrease due to the lateral inhibition existing within each nucleus (Fig. 5). On the contrary, the MSN demonstrated the slowest adaptation mainly due to the intrinsic long first-spike latency of this neuron model.

Once the network activity becomes steady, the cortex increases its activity in both channels (cortex selection onset) (Fig. 3(b)). After 25 ms, the cortex selects only one channel (which further increases the firing rate, while the other one returns to the basal level of firing) (Fig. 3(b)). This channel selection in the cortex produces a strong response in the BG: the selected channel increases their firing rate in the MSN and STN and inhibits, in turn, the nonselected channels (Fig. 5). However, the selected channel in the MSN shows transient phenomena by producing peaks of activity (200 ms long or less, as will be discussed later in Fig. 6(b)) due to the intrinsic properties of its neuron model, the long time constant of the NMDA receptor and the lateral inhibition. Conversely, the selected channel in the GPe and the SNr receives strong inhibition from the MSN, thus compensating for the stronger excitation from the STN and leading to a notorious reduction of the firing rate in the selected channel of the GPe and SNr (Fig. 5). Due to the recurrent loops between the GPe and STN (Fig. 1), the activity of the GPe remains unstable for 500 ms after the cortex selection onset. The output nucleus (SNr), not unexpectedly, decreases the activity for the selected channel, while the nonselected one remains with a basal level of activity (after a transient activity peak) (Fig. 5).

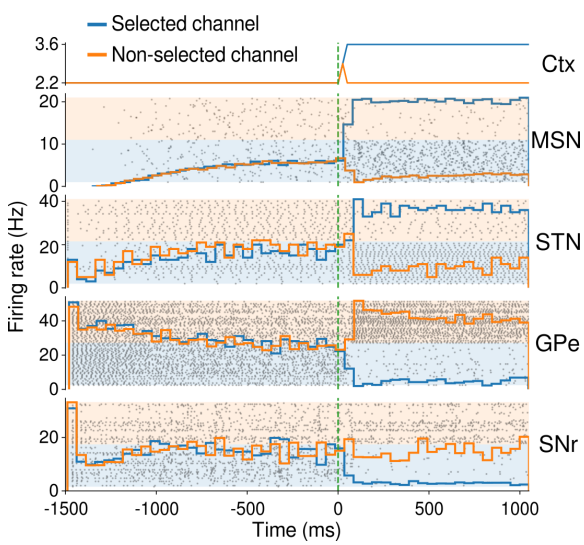

Fig. 5. (Color online) General network behavior. Raster plot (black dots) and population firing rates (solid lines) for the cortex (Ctx), MSN, STN, GPe and SNr populations. Selected and nonselected channels are, respectively, drawn with blue and orange background/line colors.

The commented network operation is valid for the control case (default DA and no HD affectation). We also tested the network with different levels of DA or HD. Increased DA levels in the model resulted in enhanced response of the MSN to the cortical input, as previously reported in freely moving rats.[59] In addition to this, the firing rates obtained for control and pathological HD MSNs are in agreement with the experimental results obtained from mice.[60] We used our model to explore if altered levels of DA and the presence of HD affectation may change the balance between excitation and inhibition in any network layer and, as a consequence, if they produce enhanced/reduced levels of selectivity in the MSN and distinctiveness in the SNr.

3.4. *Striatum (MSN) activity*

Overall, our simulations demonstrated that increase in either DA levels or noteworthy HD affectation (or both conditions together) resulted in enhanced levels of MSN activation (Fig. 6(a) green, orange and purple solid lines in the top plot) and the rest of the BG nuclei, resulting in different balances of excitation/inhibition depending on the particular configuration.

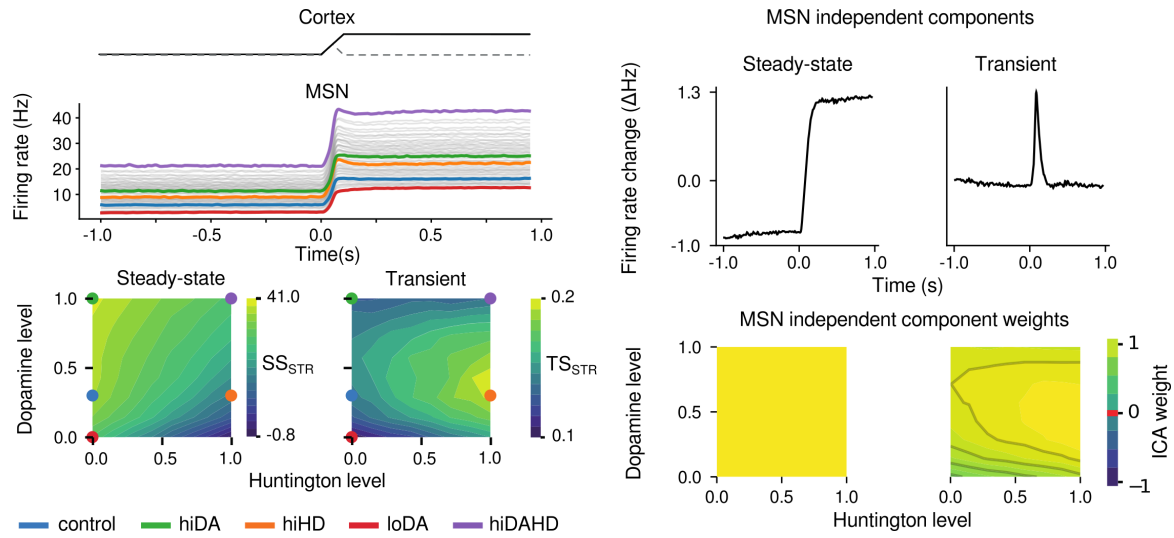

(a) (b)

Fig. 6. (Color online) Effect of different DA levels and HD conditions in the MSN. (a) (Top) Average firing rate of the selected channel in the MSN. Each trace represents a different setting, while some representative conditions have been highlighted in colors: control (default DA level and no HD) (blue), hiHD (default DA and high HD) (orange), hiDA (high DA and no HD) (green), loDA (low DA and no HD) (red) and hiDAHD (high DA and HD) (purple). (Bottom) Steady-state (SS_{MSN}) (left) and transient (TS_{MSN}) (right) selectivity within the studied parameter space (DA versus HD level). Colored circles mark the cases previously considered. (b) (Top) Independent components obtained from the MSN firing histogram by using the ICA algorithm over all the experimental conditions. (Bottom) Weight of each signal component in each experimental condition as obtained from the ICA algorithm.

In order to achieve a fuller understanding of the functional effect that altered DA and HD levels produce in the processing layers of the BG, we simulated a whole set of different configurations of the network to perform Beste's task. For each experimental condition, the activity histogram of the selected channel in the MSN has been extracted (top plot in Fig. 6(a)) and the steady-state and the transient-state selectivity have been analyzed (bottom plots in Fig. 6(a)). As a general rule, steady-state selectivity is enhanced by increased DA levels while HD affectation reduces it. On the other hand, transient selectivity is increased by HD affectation and shows an inverted "U" relationship with DA levels (medium DA levels resulted in increased transient selectivity).

Aiming to discriminate the effect of DA and HD in the emergence of steady or transient components of activity, we applied the ICA algorithm on the activity histograms of the selected channel in the MSN, resulting in the two components indicated in the top row plots in Fig. 6(b). The first component (left plot) represents a steady signal (corresponding with the steady state before and after stimulus onset), while the second component (right plot) shows transient behavior around the stimulus onset. By exploring the weights associated to each component for each experimental condition, the first component is similarly present in all the experimental conditions, while the second component shows differences among the configurations (bottom row in Fig. 6(b)). The second component is more prominent with high HD affectation and medium DA levels.

3.5. *Substantia nigra (SNr) activity*

Similarly, as previously analyzed in the MSN, we have explored the averaged firing activity of the SNr (Fig. 7(a)) in response to the cortex input activity that mimics the stimulation received during Beste's task. Moreover, we have also analyzed the distinctiveness[34] of the stimulus with different network conditions (DA and HD levels). The results show that both the transient and the steady-state distinctiveness increase with high levels of DA and reduced HD affectation.

We also used ICA in the SNr signals, obtaining three independent components able to explain at least the 90% of the variability of the original signal.

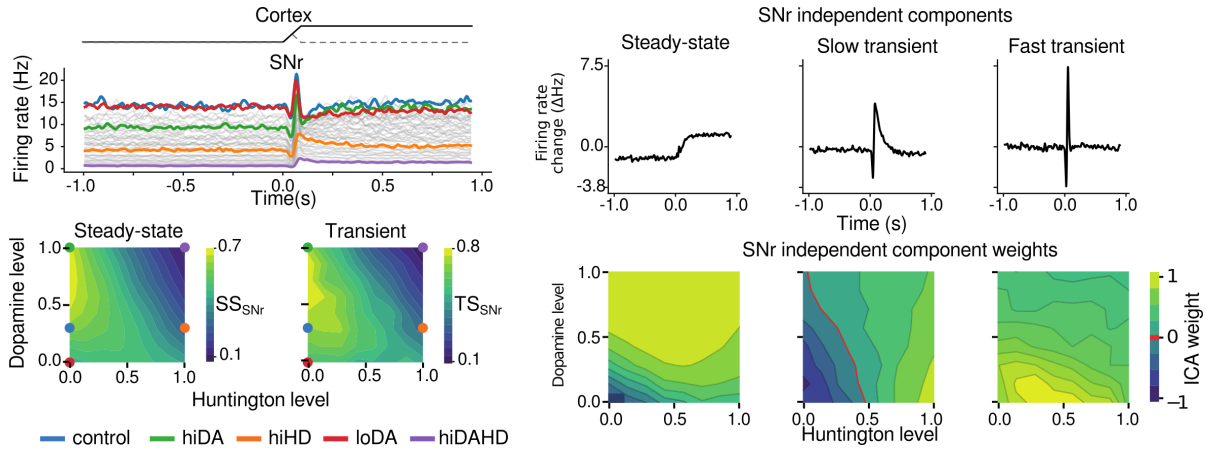

(a) (b)

Fig. 7. (Color online) Effect of different DA levels and HD conditions in the SNr. (a) (Top) Average firing rate of the nonselected channel in the SNr. Each trace represents a different setting, while some representative conditions have been highlighted in colors: control (default DA level and no HD) (blue), hiHD (default DA level and high HD) (orange), hiDA (high DA level and no HD) (green), loDA (low DA level and no HD) (red) and hiDAHD (high DA level and HD) (purple). (Bottom) Steady-state (left) and transient (right) distinctiveness in the SNr within the parameters space studied (DA versus HD level). Colored circles mark the cases previously considered. (b) (Top) Independent components obtained from the SNr firing histogram by using the ICA algorithm over all the experimental conditions. (Bottom) Weight of each signal component in each experimental condition as obtained from the ICA algorithm.

Figure 7(b) shows the extracted independent components and their corresponding weights for each experimental condition. The first component is associated to the steady-state evolution, while the other two are related to the transient phenomena (slow and fast). The distribution of the weights of these components shows very distinct patterns. While the steady-state and slow-transient components show some linearity (the first with DA level and the second with HD level), the fast-transient component shows a nonlinear behavior, with more weight when the DA level is low and the HD level is medium.

4. Discussion

4.1. *Interpretation of results*

The obtained results are in agreement with previous research. Reference 1 showed that the potentiation of the transient component explains (at least, partially) why HD patients achieve better performance in timed decision tasks. This effect was previously explained as enhanced information processing in simple sensorimotor tasks. By using ICA, we have evidenced neuronal correlates of this experimental performance improvement resulting from increased DA levels in healthy subjects receiving levodopa.[9] Specifically, the transient independent component detected at MSN is more prominent with high HD affectation and medium DA levels.

Regarding the SNr activity, both the steady-state and the transient distinctiveness fail to explain the enhanced performance of HD patients in Beste's task. Although previous papers in the literature have associated this paradoxical improvement to the alteration of the selectivity in the MSN, our simulations demonstrate that increased selectivity does not propagate to the subsequent SNr layer (the output nucleus of the BG). By studying the independent components obtained from the activity histograms we are able to offer an alternative explanation to this paradoxical improvement. After observing the shape of each component (bottom plots in Fig. 7(b)), we have concluded that these components can propagate from the MSN to the SNr. The weight of each component for each experimental condition indicates which circumstances facilitate the propagation of the corresponding component (e.g. while the slow-transient component reliably propagates with high HD, the fast-transient component more consistently propagates with medium HD and low–medium DA). Thus,

the propagation of the fast-transient component from the MSN to the SNr may support the paradoxical improvement in Beste's task observed in patients in the early stages of HD.

4.2. *Comparison with previous studies*

To date, several BG computational models have been proposed for different purposes. A detailed[27] and a subsequently simplified[28] computational model expressing the DA modulation in MSN D1 and D2 were proposed, and then added to a three-dimensional network model together with fast spiking interneurons (FSI) in the striatum.[29] Other models studied the exploration/exploitation trade-off,[8,30,61,62] or reproduced diverse behavioral tasks with a complex model containing several neuronal nuclei (cortex, BG and thalamus).[63] In some models, phasic DA signals have been added on top of a tonic DA value, reproducing the neural mechanism for which the triggering of a movement requires a dopaminergic burst just preceding the movement onset.[64,65] There are studies, more focused on HD, as in Ref. 1, where they studied the origin of HD paradoxical effects as a consequence of the alteration of the transient selectivity in the MSN.

The general behavior of the MSN population has been evaluated against selectivity metrics previously proposed in the literature.[1] According to these metrics, high levels of HD affectation present contradictory effects (decrease and increase) in steady-state and transient-state selectivity, in agreement with previous simulations. These results confirm the prediction that the transient-state selectivity metric in the MSN may explain the paradoxical speed improvement in Beste's task by HD patients,[14] assuming that middle levels of HD in our model correspond to the early stages of HD patients.[10,66] Although our simulations support this prediction, the evaluation of similar metrics in the subsequent layer (the SNr) indicates that the transient distinctiveness does not reflect the paradoxical behavioral improvement in HD patients. However, the analysis of the components extracted by the ICA algorithm in the SNr activity (the BG output layer) evidenced two transient components and one steady component. The weights of the components in HD conditions indicate that only the fastest component supports the paradoxical speed improvement in Beste's task. This component would act by abruptly avoiding the activity of alternative behavioral options.

Our computational model also allowed the analysis of tonic DA effect on BG operation. Previous studies did not specifically address the effect of DA in steady-state or transient-state selectivity (e.g. Ref. 1 included DA in the computational model of HD but with a fixed value throughout all experimental conditions). In our simulations, only the transient-state metric in the MSN evidenced decremented selectivity caused by high or low (nonmedium) DA levels. According to these simulations, medium levels of DA may improve the subject's performance in selection tasks. Similar metrics in the SNr show enhanced steady-state and transient distinctiveness linked to higher levels of DA. These results are supported by the cognitive improvement registered in behavioral tasks by subjects receiving levodopa.[9] The ICA algorithm used on the SNr signals shows that transient components also occur in the SNr for high HD affectation (slow component) or a combination of medium HD affectation and low DA levels (fast component). These results explain how the augmented transient selectivity associated to the MSN of HD patients propagates to the SNr, projecting to the cortex through the thalamus and originating behavioral effects.

The application of the ICA algorithm in the SNr also evidences how different conditions affect each component of the signal. The steady-state component mainly depends on DA level, making this component a candidate for a nonpathological improvement mechanism in performance during selection tasks. It is in agreement with the experimental improvement of healthy subjects with high DA levels in selection tasks.[9] The slow-transient component is affected by the HD affectation but not by DA levels while the fast-transient component requires medium–low levels of DA and medium levels of HD affectation. Since paradoxical improvement on HD patients requires medium levels of HD affectation[14] and low or normal levels of DA, the fast-transient component closely fits this experimentally observed pattern. Thus, this fast component could be considered as a plausible marker for sensorial discrimination performance. Our model is also compatible with the reported deterioration of HD patients treated with levodopa,[13] where high HD and DA levels would deteriorate performance as the fast-transient

component is reduced. In any case, further experimental studies are required in order to validate this hypothesis.

4.3. *Model limitations and future work*

One of the main limitations of the proposed model is that it lacks the recurrent loop between the BG and the cortex (where the decision process is thought to take place) through the thalamus. In absence of the cortico-BG-thalamic-cortical loop, our model is assuming a simple cause-effect relationship between the cortex and the BG. Current research considers a system-level approach where specific behaviors are generated by the interplay of different subsets of components of the brain.[67–69] The BG is not making the decision in isolation as the cortex is also taking part in this process: cortical feedback projections to the striatum and STN make the internal competition between channels a cumulative dynamical process.[70] Because of this, our result analysis is restricted to a small time window around the stimulus (before the re-entrant signal from the cortex is able to affect the BG activity). This time window is wide enough to allow us to explore the propagation of the transient components through a more extensive model of the BG than any previous research. Integrating the whole closed-loop is key in future research, as recently proposed.[64,65] The inclusion of cortical processing structures in a closed-loop could facilitate further understanding of larger-timescale motor phenomena, such as the mechanisms of event-related desynchronization/synchronization found during motor imagery tasks.[71]

For the sake of simplicity of the analyses carried out in this study, we just took into account the tonic DA signals in our simulations (phasic DA signals were simplified). Future approaches should address how phasic DA signals might unbalance the state of equilibrium between the direct and indirect pathways.[64,65,70] Moreover, the presence of DA-dependent plasticity[26,31] in the cortex-MSN connections may somehow affect the BG processing of the incoming decisions. Nevertheless, the proposed model does not consider learning at any level (cortical or sub-cortical). Our simulations assumed the subject had previously learnt the action selection task and it was on the automatization phase in which the cortex-striatum network plays a pivotal role.[72]

Although interneurons in the striatum (and specifically the FSI) shape the activity of the MSN,[36] and other models in the literature have already included these type of neurons,[1,34,35] we have avoided including these kinds of neurons as our preliminary simulations have shown no relevant effect for our particular behavioral task. This might happen due to the relatively low levels of input activity we have used in our experiments. The FSI show a stronger influence when a higher baseline and stepped inputs are used.[1]

Finally, one possible use of the components found in this study is to help us understand the origin of neurophysiology data obtained in real behavioral experiments. In Ref. 14, HD patients and controls were required to differentiate between short and long tones (a task very similar to the one simulated in this paper) while an EEG was recording the brain activity. They found that the paradoxical behavioral improvement (reflected as better accuracy and faster time responses in HD patients) correlated with the intensity of an event-related potential (ERP) signal obtained in the EEG known as mismatch negativity (MMN). This ERP signal could indicate the recognition of unexpected events by the auditory system.[14] Specifically, its presence can be measured in an EEG as a negative peak around 100 ms after the stimulus presentation. This timing precisely matches the propagation of the fast-transient component from the cortex to the SNr ($\sim$70 ms after the stimulus presentation according to the ICA algorithm) plus the transmission delay from the SNr to the cortex through the thalamus, which has been estimated around 35 ms.[73–75] In any case, additional research with computational models (possibly including thalamic and cortical areas in the loop with BG) is required to better understand this process.

5. Conclusion

In this paper, we propose a new analysis method for evaluating transient phenomena, and it has been applied to the activity of BG populations in the framework of a detailed computational model. These novel metrics allow the explicit assessment of how cortical activity is transferred to the thalamus through the BG. We have analyzed how the relevant independent components of the signals in the input and output layers of the BG are affected with

HD affectation and tonic DA levels. This combined study of DA and HD represents an innovative contribution, explaining the nonmonotonic relationship between DA/HD levels and the selectivity of the BG. This paper describes the complex relations between BG neuronal populations that are in accordance with the behavioral results that have been observed in the literature.

Acknowledgments

This research is supported by the University of Granada under FEDER 2014–2020, by the Anda lucía Regional funds under the Grants EmbBrain (A-TIC-276-UGR18) and CEREBIO (FEDER-P18-FR-2378) and National Grant (MICINN-FEDER-PID2019-109991GB-I00). This research has also received funding from the EU H2020 Framework Program under the Specific Grant Agreement No. 945539 (Human Brain Project SGA3). Additionally, the main author has been funded with a national research training Grant (FPU17/04432). Finally, the 3D character model used to illustrate this paper is taken from Adobe's Mixamo platform.

Appendix A. Neuron Models

All the neurons included in our BG model have been simulated using different versions of the Izhikevich neuron model. This model is computationally very efficient and allows the reproduction of all the firing patterns previously described in the BG.[28,33] According to the Izhikevich model, the membrane potential v of the neuron is updated according to the following equation:

$$C\frac{dv}{dt} = k(v - v_r)(v - v_t) - u + I, \tag{A.1}$$

where I is the total synaptic input (defined below), C is the membrane capacitance, v_r is the resting potential, v_t is the instantaneous threshold potential, k is an abstract parameter that regulates the influence of the current membrane potential value in its derivative and u is a recovery parameter updated by in the following equation:

$$\frac{du}{dt} = a(b(v - v_r) - u), \tag{A.2}$$

where a sets the time scale of the recovery variable with low values corresponding to slow recoveries, and b describes the sensitivity of the recovery variable to fluctuations of the membrane potential.

An action potential is elicited in this model when the firing threshold (v_{peak}) is exceeded by the membrane potential v. In this case, the variables in the model are updated according to the following equation:

$$v \leftarrow c; \quad u \leftarrow u + d, \tag{A.3}$$

where c is the voltage reset value and d is the reset of the recovery variable.

All the neuron sub-types defined in the MSN (D1 and D2), GPe (A, B and C) and SNr can be implemented using the original Izhikevich neuron model. On the contrary, the three neuron sub-types of the STN show different responses after long depolarization, including RB, LLRS and NR. These effects have been modeled by extending the original Izhikevich's equations with one additional recovery variable (u_2).[62] The state variables are updated according to the following differential equations:

$$C\frac{dv}{dt} = k(v - v_r)(v - v_t) - u_1 - w_2 \cdot u_2 + I, \tag{A.4}$$

$$\frac{du_1}{dt} = a_1(b_1(v - v_r) - u_1), \tag{A.5}$$

$$\frac{du_2}{dt} = a_2(Gb_2(v - v_{r2}) - u_2), \tag{A.6}$$

where one additional recovery variable (u_2) and its parameters (a_1, a_2, b_1, b_2, d_1, d_2, w_1, w_2, G and U) have been added to account for the previously described behavior without losing the basic repertoire of firing patterns supported by the basic recovery variable u_1.[34,76] For the NR neurons, G is set to 1, while for RB and LLRS neurons, $G = H(v_{r2} - v)$ is the Heaviside step function:

$$H(x) = \begin{cases} 0, & x < 0, \\ \dfrac{1}{2}, & x = 0, \\ 1, & x > 0. \end{cases} \tag{A.7}$$

When the membrane potential moves above the adaptive firing threshold ($v \geq v_{\text{peak}} + Uu_2$) the model variables are set as indicated in the following expressions:

$$v = c - Uu_2, \tag{A.8}$$

$$u_1 = u_1 + d_1, \tag{A.9}$$

$$u_2 = u_2 + d_2. \tag{A.10}$$

Finally, at high firing rates, u_2 may increase dramatically. To avoid this phenomenon, the U value is defined according to the following expression:

$$U = \frac{1}{w_1|u_2| + \frac{1}{w_1}}. \tag{A.11}$$

The value of all these neuron model parameters for each cell type can be found in Tables 2–4 in https://github.com/EduardoRosLab/BG_selectivity/raw/master/parameters_tables.pdf.

Appendix B. Synapse Models

The input current (I) targeting a neuron is defined as follows[29]:

$$I = I_{\text{AMPA}} + I_{\text{NMDA}} B(v) + I_{\text{GABA}}. \tag{B.1}$$

I_{AMPA}, I_{NMDA} and I_{GABA} are current inputs from AMPA, NMDA and GABA receptors, and $B(v)$ is a term that models the voltage-dependent magnesium plug in the NMDA receptors[46] as follows:

$$B(v) = \frac{1}{1 + \frac{[Mg^{2+}]_0}{3.57} e^{-0.062v}}, \tag{B.2}$$

where $[Mg^{2+}]_0$ is the equilibrium concentration of magnesium ions. The input current of each channel z is defined as follows:

$$I_z = y_z(E_z - v), \tag{B.3}$$

where y_z is a exponentially-decaying conductance representing the contribution of receptor z to the membrane potential, E_z is reversal potential of receptor z and v is the current membrane potential of the neuron.

The value of all these synaptic parameters can be found in Table 1 in https://github.com/EduardoRosLab/BG_selectivity/raw/master/parameters_tables.pdf.

Appendix C. Dopaminergic Modulation Model

In the MSN, the overall *in vivo* effect of the DA receptors D1 and D2 is that the stimulation of the D1 receptors increases neuron excitability, while the stimulation of the D2 receptors decrements the neuron firing,[77] as expressed in Eqs. (C.1) and (C.2). There are also neuromodulatory effects implemented following Refs. 1, 29 and 27, where da represents the global level of DA in the system. This influences the D1 and D2 DA receptors according to the neuromodulatory factors β_1 and β_2, respectively. Equation (C.3) models the D1-receptor mediated enhancement of the inward-rectifying potassium current. Equation (C.4) models the enhancement of the L-type Ca2+ current. Finally, Eq. (C.5) models the increased sensitivity to injection current following D2 activation:

$$I_{\text{NMDA}} \leftarrow I_{\text{NMDA}}(1 + \beta_1 \cdot \text{da}), \tag{C.1}$$

$$I_{\text{AMPA}} \leftarrow I_{\text{AMPA}}(1 - \beta_2 \cdot \text{da}), \tag{C.2}$$

$$v_r \leftarrow v_r(1 + \beta_1 \cdot \text{da}), \tag{C.3}$$

$$d \leftarrow d(1 - \beta_2 \cdot \text{da}), \tag{C.4}$$

$$k \leftarrow k(1 - \beta_1 \cdot \text{da}). \tag{C.5}$$

GPe and STN neurons also show DA neuromodulatory effects on their synaptic receptors, which have been modeled as follows:

$$I_{\text{AMPA}} \leftarrow I_{\text{AMPA}}(1 - \beta_1 \cdot \text{da}), \tag{C.6}$$

$$I_{\text{NMDA}} \leftarrow I_{\text{NMDA}}(1 - \beta_1 \cdot \text{da}), \tag{C.7}$$

$$I_{\text{GABA}} \leftarrow I_{\text{GABA}}(1 - \beta_2 \cdot \text{da}). \tag{C.8}$$

The value of all these dopaminergic modulation parameters for each cell type can be found in Tables 2–4 in https://github.com/EduardoRosLab/BG_selectivity/raw/master/parameters_tables.pdf.

References

1. A. Tomkins, E. Vasilaki, C. Beste, K. Gurney and M. D. Humphries, Transient and steady-state selection in the striatal microcircuit, *Front. Comput. Neurosci.* **7** (2014) 192.
2. O. Hikosaka, Y. Takikawa and R. Kawagoe, Role of the basal ganglia in the control of purposive saccadic eye movements, *Phys. Rev.* **80**(3) (2000) 953–978.
3. P. Redgrave, T. J. Prescott and K. Gurney, The basal ganglia: A vertebrate solution to the selection problem? *Neuroscience* **89**(4) (1999) 1009–1023.
4. S. Shipp, The functional logic of corticostriatal connections, *Brain Struct. Funct.* **222** (2017) 669–706.
5. M. D. Humphries, R. D. Stewart and K. N. Gurney, A physiologically plausible model of action selection and oscillatory activity in the basal ganglia, *J. Neurosci.* **26**(50) (2006) 12921–12942.
6. K. Gurney, T. J. Prescott and P. Redgrave, A computational model of action selection in the basal ganglia. I. A new functional anatomy, *Biol. Cybern.* **84** (2001) 401–410.
7. K. Gurney, T. J. Prescott and P. Redgrave, A computational model of action selection in the basal ganglia. II. Analysis and simulation of behavior, *Biol. Cybern.* **84** (2001) 411–423.

8. S. M. Suryanarayana, J. H. Kotaleski, S. Grillner and K. N. Gurney, Roles for globus pallidus externa revealed in a computational model of action selection in the basal ganglia, *Neural Netw.* **109** (2019) 113–136.
9. P. Rihet, C. A. Possamaï, J. Micallef-Roll, O. Blin and T. Hasbroucq, Dopamine and human information processing: A reaction-time analysis of the effect of levodopa in healthy subjects, *Psychopharmacology* **163**(1) (2002) 62–67.
10. M. Nance, J. S. Paulsen, A. Rosenblatt and V. Wheelock, *A Physician's Guide to the Management of Huntington's Disease*, 3rd edn. (Huntington's Disease Society of America, 2011).
11. M. F. Beal and R. J. Ferrante, Experimental therapeutics in transgenic mouse models of Huntington's disease, *Nat. Rev. Neurosci.* **5** (2004) 373–384.
12. Y. Deng, R. Albin, J. Penney, A. Young, K. Anderson and A. Reiner, Differential loss of striatal projection systems in Huntington's disease: A quantitative immunohistochemical study, *J. Chem. Neuroanat.* **27** (2004) 143–164.
13. C. Loeb, G. G. L. M. Roccatagliata, G. La Medica, G. Abbruzzese and C. Albano, Levodopa and Huntington's chorea *J. Neurol. Neurosurg. Psychiatry*, **39**(10) (1976) 958–961.
14. C. Beste, C. Saft, O. Gunturkun and M. Falkenstein, Increased cognitive functioning in symptomatic huntington's disease as revealed by behavioral and event-related potential indices of auditory sensory memory and attention, *J. Neurosci.* **28** (2008) 11695–11702.
15. J. Sorinas, M. D. Grima, J. M. Ferrandez and E. Fernandez, Identifying suitable brain regions and trial size segmentation for positive/negative emotion recognition, *Int. J. Neural Syst.* **29** (2019) 1850044.
16. J. Gomez-Pilar, J. Poza, A. Bachiller, C. Gómez, P. Núñez, A. Lubeiro, V. Molina and R. Hornero, Quantification of graph complexity based on the edge weight distribution balance: Application to brain networks, *Int. J. Neural Syst.* **28** (2018) 1750032.
17. S. Ghosh-Dastidar and H. Adeli, Spiking neural networks, *Int. J. Neural Syst.* **19**(4) (2009) 295–308.
18. S. Ghosh-Dastidar and H. Adeli, Improved spiking neural networks for eeg classification and epilepsy and seizure detection, *Integr. Comput.-Aided Eng.* **14**(3) (2007) 187–212.
19. S. Ghosh-Dastidar and H. Adeli, A new supervised learning algorithm for multiple spiking neural networks with application in epilepsy and seizure detection, *Neural Netw.* **22**(10) (2009) 1419–1431.
20. A. Geminiani, C. Casellato, A. Antonietti, E. D. Angelo and A. Pedrocchi, A multiple-plasticity spiking neural network embedded in a closed-loop control system to model cerebellar pathologies, *Int. J. Neural Syst.* **28**(5) (2018) 1750017.
21. G. Antunes, S. F. Faria da Silva and F. M. Simoes de Souza, Mirror neurons modeled through spike-timing-dependent plasticity are affected by channelopathies associated with autism spectrum disorder, *Int. J. Neural Syst.* **28**(5) (2018) 1750058.
22. A. Antonietti, J. Monaco, E. D'Angelo, A. Pedrocchi and C. Casellato, Dynamic redistribution of plasticity in a cerebellar spiking neural network reproducing an associative learning task perturbed by tms, *Int. J. Neural Syst.* **28**(9) (2018) 1850020.
23. C. Liu, J. Wang, Y. Y. Chen, B. Deng, X. L. Wei and H. Y. Li, Closed-loop control of the thalamocortical relay neuron's Parkinsonian state based on slow variable, *Int. J. Neural Syst.* **23**(4) (2013) 1–14.
24. F. Su, J. Wang, B. Deng, X. L. Wei, Y. Y. Chen, C. Liu and H. Y. Li, Adaptive control of Parkinson's state based on a nonlinear computational model with unknown parameters, *Int. J. Neural Syst.* **25**(1) (2015) 1–13.
25. T. C. Stewart *et al.*, Dynamic behavior of a spiking model of action selection in the basal ganglia, in *Proc. 10th Int. Conf. Cognitive Modeling* (Drexel University, Philadelphia, 2010), pp. 235–240.
26. T. C. Stewart, T. Bekolay and C. Eliasmith, Learning to select actions with spiking neurons in the basal ganglia, *Front. Neurosci.* **6** (2012) 1–14.
27. J. T. Moyer, J. A. Wolf and L. H. Finkel, Effects of dopaminergic modulation on the integrative properties of the ventral striatal medium spiny neuron, *J. Neurophysiol.* **98** (2007) 3731–3748.
28. M. Humphries, Capturing dopaminergic modulation and bimodal membrane behavior of striatal medium spiny neurons in accurate, reduced models, *Front. Comput. Neurosci.* **3** (2009) 1–16.
29. M. D. Humphries, R. Wood and K. Gurney, Dopamine-modulated dynamic cell assemblies generated by the GABAergic striatal microcircuit, *Neural Netw.* **22**(8) (2009) 1174–1188.
30. Z. Fountas and M. Shanahan, The role of cortical oscillations in a spiking neural network model of the basal ganglia, *Plos One* **12** (2017) e0189109.
31. K. N. Gurney, M. D. Humphries and P. Redgrave, A new framework for cortico-striatal plasticity: Behavioral theory meets *in vitro* data at the reinforcement-action interface, *PLoS Biol.* **13**(1) (2015) 1–25.
32. S. Kunkel, A. Morrison, P. Weidel, J. M. Eppler, A. Sinha, W. Schenck, M. Schmidt, S. B. Vennemo, J. Jordan, A. Peyser, D. Plotnikov, S. Graber, T. Fardet, D. Terhorst, H. Mørk, G. Trensch, A. Seeholzer, R. Deepu, J. Hahne, I. Blundell, T. Ippen, J. Schuecker, H. Bos, S. Diaz, E. Hagen, S. Mahmoudian, C. Bachmann, M. E. Lepperød, O. Breitwieser, B. Golosio, H. Rothe, H. Setareh, M. Djurfeldt, T. Schumann, A. Shusharin, J. Garrido, E. B.

Muller, A. Rao, J. H. Vieites and H. E. Plesser, Hans Ekkehard (2017, March 1). NEST 2.12.0. Zenodo, http://doi.org/10.5281/zenodo.259534.

33. E. M. Izhikevich, *Dynamical Systems in Neuroscience*: *The Geometry of Excitability and Bursting* (The MIT Press, 2005).
34. Z. Fountas, Action selection in the rhythmic brain: The role of the basal ganglia and tremor, Ph.D. thesis, Imperial College London (2016), pp. 224–228.
35. M. D. Humphries, R. Wood and K. Gurney, Reconstructing the three-dimensional GABAergic microcircuit of the striatum, *PLoS Comput. Biol.* **6** (2010) 1–16.
36. T. Koós and J. M. Tepper, Inhibitory control of neostriatal projection neurons by GABAergic interneurons, *Nat. Neurosci.* **2**(5) (1999) 467–472.
37. D. F. English, O. Ibanez-Sandoval, E. Stark, F. Tecuapetla, G. Buzsáki, K. Deisseroth, J. M. Tepper and T. Koos, GABAergic circuits mediate the reinforcement-related signals of striatal cholinergic interneurons, *Nat. Neurosci.* **15**(1) (2012) 123–130.
38. M. R. DeLong, Activity of basal ganglia neurons during movement, *Brain Res.* **40** (1972) 127–135.
39. J. Bugaysen, M. Bronfeld, H. Tischler, I. Bar-Gad and A. Korngreen, Electrophysiological characteristics of globus pallidus neurons, *PLoS One* **5** (2010) e12001.
40. N. E. Hallworth, C. J. Wilson and M. D. Bevan, Apamin-sensitive small conductance calcium-activated potassium channels, through their selective coupling to voltage-gated calcium channels, are critical determinants of the precision, pace, and pattern of action potential generation in rat subthalamic Nu, *J. Neurosci.* **23** (2003) 7525–7542.
41. H. Nakanishi, A. Tamura, K. Kawai and K. Yamamoto, Electrophysiological studies of rat substantia nigra neurons in an *in vitro* slice preparation after middle cerebral artery occlusion, *Neuroscience* **77** (1997) 1021–1028.
42. F.-M. Zhou and C. Lee, Intrinsic and integrative properties of substantia nigra pars reticulata neurons, *Neuroscience* **198** (2011) 69–94.
43. C. R. Lee and J. M. Tepper, Morphological and physiological properties of parvalbumin- and calretinin-containing γ-aminobutyric acidergic neurons in the substantia nigra, *J. Comp. Neurol.* **500** (2007) 958–972.
44. M. Lindahl, I. Kamali Sarvestani, O. Ekeberg and J. H. Kotaleski, Signal enhancement in the output stage of the basal ganglia by synaptic short-term plasticity in the direct, indirect, and hyperdirect pathways, *Front. Comput. Neurosci.* **7** (2013) 76.
45. H. Nakanishi, H. Kita and S. Kitai, Intracellular study of rat substantia nigra pars reticulata neurons in an *in vitro* slice preparation: Electrical membrane properties and response characteristics to subthalamic stimulation, *Brain Res.* **437** (1987) 45–55.
46. C. E. Jahr and C. F. Stevens, Voltage dependence of NMDA-activated predicted by single-channel kinetics, *J. Neurosci.* **10**(9) (1990) 3178–3182.
47. M. M. Fan and L. A. Raymond, N-Methyl-d-aspartate (NMDA) receptor function and excitotoxicity in Huntington's disease, *Prog. Neurobiol.* **81**(5–6) (2007) 272–293.
48. J. W. Goodliffe, H. Song, A. Rubakovic, W. Chang, M. Medalla, C. M. Weaver and J. I. Luebke, Differential changes to D1 and D2 medium spiny neurons in the 12-month-old Q175+/− mouse model of Huntington's Disease, *PLoS One* **13** (2018) e0200626.
49. A. J. McGeorge and R. L. Faull, The organization of the projection from the cerebral cortex to the striatum in the rat, *Neuroscience* **29**(3) (1989) 503–537.
50. T. Moriizumi and T. Hattori, Pyramidal cells in rat temporoauditory cortex project to both striatum and inferior colliculus, *Brain Res. Bull.* **27**(1) (1991) 141–144.
51. X. Guo, H. Yu, N. X. Kodama, J. Wang and R. F. Galán, Fluctuation scaling of neuronal firing and bursting in spontaneously active brain circuits, *Int. J. Neural Syst.* **30**(1) (2020) 1950017.
52. G. Cantwell, M. Riesenhuber, J. L. Roeder and F. G. Ashby, Perceptual category learning and visual processing: An exercise in computational cognitive neuroscience, *Neural Netw.* **89** (2017) 31–38.
53. M. J. Frank, By carrot or by stick: Cognitive reinforcement learning in parkinsonism, *Science* **306** (2004) 1940–1943.
54. H. Schroll, J. Vitay and F. H. Hamker, Working memory and response selection: A computational account of interactions among cortico-basalganglio-thalamic loops, *Neural Netw.* **26** (2012) 59–74.
55. Z. Fountas and M. Shanahan, Assessing selectivity in the basal ganglia: The "gearbox" hypothesis, *bioRxiv* (2017), doi:10.1101/197129
56. E. Oja and A. Hyva, Independent component analysis: Algorithms and applications, *Neural Networks* **13**(4–5) (2000) 411–430.
57. F. Pedregosa, G. Varoquaux, A. Gramfort, V. Michel, B. Thirion, O. Grisel, M. Blondel, P. Prettenhofer, R. Weiss, V. Dubourg, J. Vanderplas, A. Passos, D. Cournapeau, M. Brucher, M. Perrot and E. Duchesnay, Scikit-learn: Machine learning in Python, *J. Mach. Learn. Res.* **12** (2011) 2825–2830.
58. R. Schmidt, D. K. Leventhal, N. Mallet, F. Chen and J. D. Berke, Canceling actions involves a race between basal ganglia pathways, *Nat. Neurosci.* **16**(8) (2013) 1118.
59. R. Natarajan and B. K. Yamamoto, The basal ganglia as a substrate for the multiple actions of amphetamines, *Basal Ganglia* **1** (2011) 49–57.

60. B. R. Miller, A. G. Walker, A. S. Shah, S. J. Barton and G. V. Rebec, Dysregulated information processing by medium spiny neurons in striatum of freely behaving mouse models of huntington's disease, *J. Neurophysiol.* **100** (2008) 2205–2216.
61. S. Devarajan, P. S. Prashanth and V. S. Chakravarthy, The role of the basal ganglia in exploratory behavior in a model based on reinforcement learning, *Lect. Notes Comput. Sci. Including Subseries Lect. Notes Artif. Intell. and Lect. Notes Bioinf.* **3316**(2) (2004) 70–77.
62. Z. Fountas and M. Shanahan, Phase offset between slow oscillatory cortical inputs influences competition in a model of the basal ganglia, *2014 Int. Joint Conf. Neural Networks* (*IJCNN*) (IEEE, July 2014), pp. 2407–2414.
63. C. Eliasmith, T. C. Stewart, X. Choo, T. Bekolay, T. DeWolf, C. Tang, D. Rasmussen, Y. Tang, C. Tang and D. Rasmussen, A large-scale model of the functioning brain, *Science* **338**(6111) (2012) 1202–1205.
64. D. Caligiore, F. Mannella, M. A. Arbib and G. Baldassarre, Dysfunctions of the basal ganglia-cerebellar-thalamo-cortical system produce motor tics in Tourette syndrome, *PLoS Comput. Biol.* **13** (2017) e1005395.
65. D. Caligiore, F. Mannella and G. Baldassarre, Different dopaminergic dysfunctions underlying Parkinsonian Akinesia and tremor, *Front. Neurosci.* **13** (2019) 1–15.
66. J.-P. Vonsattel, R. H. Myers, T. J. Stevens, R. J. Ferrante, E. D. Bird and E. P. Richardson, Neuropathological classification of huntington's disease, *J. Neuropathol. Exp. Neurol.* **44** (1985) 559–577.
67. D. Caligiore and M. H. Fischer, Vision, action and language unified through embodiment, *Psychol. Res.* **77**(1) (2013) 1–6.
68. D. Caligiore, G. Pezzulo, G. Baldassarre, A. C. Bostan, P. L. Strick, K. Doya, R. C. Helmich, M. Dirkx, J. Houk, H. Jörntell, A. Lago-Rodriguez, J. M. Galea, R. C. Miall, T. Popa, A. Kishore, P. F. M. J. Verschure, R. Zucca and I. Herreros, Consensus paper: Towards a systems-level view of cerebellar function: The interplay between cerebellum, basal ganglia, and cortex, *Cerebellum* **16** (2017) 203–229.
69. D. Caligiore, M. A. Arbib, R. C. Miall and G. Baldassarre, The super-learning hypothesis: Integrating learning processes across cortex, cerebellum and basal ganglia, *Neurosci. Biobehav. Rev.* **100** (2019) 19–34.
70. F. Mannella and G. Baldassarre, Selection of cortical dynamics for motor behavior by the basal ganglia, *Biol. Cybern.* **109**(6) (2015) 575–595.
71. F. Li, W. Peng, Y. Jiang, L. Song, Y. Liao, C. Yi, L. Zhang, Y. Si, T. Zhang, F. Wang, R. Zhang, Y. Tian, Y. Zhang, D. Yao and P. Xu, The dynamic brain networks of motor imagery: Time-varying causality analysis of scalp EEG, *Int. J. Neural Syst.* **29** (2019) 1850016.
72. V. B. Penhune and C. J. Steele, Parallel contributions of cerebellar, striatal and M1 mechanisms to motor sequence learning, *Behav. Brain Res.* **226**(2) (2012) 579–591.
73. P. Robinson, C. J. Rennie, D. Rowe and S. O'connor, Estimation of multiscale neurophysiologic parameters by electroencephalographic means, *Hum. Brain Mapp.* **23**(1) (2004) 53–72.
74. J. A. Roberts and P. A. Robinson, Modeling absence seizure dynamics: Implications for basic mechanisms and measurement of thalamocortical and corticothalamic latencies, *J. Theor. Biol.* **253**(1) (2008) 189–201.
75. S. J. van Albada and P. A. Robinson, Mean-field modeling of the basal ganglia-thalamocortical system. i: Firing rates in healthy and parkinsonian states, *J. Theor. Biol.* **257**(4) (2009) 642–663.
76. Z. Fountas and M. Shanahan, GPU-based fast parameter optimization for phenomenological spiking neural models, in *2015 International Joint Conference on Neural Networks* (*IJCNN*) (Killarney, 2015), pp. 1–8, doi:10.1109/IJCNN.2015.7280668.
77. A. R. West and A. A. Grace, Opposite influences of endogenous dopamine D1 and D2 receptor activation on activity states and electrophysiological properties of striatal neurons: Studies combining *in vivo* intracellular recordings and reverse microdialysis, *J. Neurosci.* **22** (2002) 294–304.